Structural behavior of the kagome antiferromagnet $TmBaCo_4O_7$: Neutron diffraction study and group-theoretical consideration

D. D. Khalyavin, L. C. Chapon, and P. G. Radaelli
ISIS Facility, Rutherford Appleton Laboratory–CCLRC, Chilton, Didcot, Oxfordshire OX11 0QX, United Kingdom

H. Zheng and J. F. Mitchell
Materials Science Division, Argonne National Laboratory, 9700 S. Cass Avenue, Argonne, Illinois 60439, USA
(Received 29 June 2009; revised manuscript received 7 September 2009; published 12 October 2009)

The first-order structural phase transition at $T_S \sim 240$ K in the extended kagome antiferromagnet $TmBaCo_4O_7$ has been studied by neutron powder diffraction. In order to comprehend the microscopic origin of the transition, a detailed symmetry analysis is performed, based on crystallographic parameters obtained by Rietveld analysis of the neutron data. The results are consistent with the $P31c \rightarrow Pna2_1$ symmetry lowering and support a displacive nature of the phase transition. The complex tilting pattern of CoO_4 tetrahedra in both triangular and kagome sublattices is described based on symmetry-adapted pseudovector distortion modes of the parent $P6_3mc$ hexagonal structure. Our analysis reveals that the unusual topology of the crystal structure does not allow CoO_4 tetrahedra to rotate as rigid units, resulting in their inevitable distortions, whatever the combination of rotational modes considered. A possible analogy between polyhedral distortions and spin frustration in this system is discussed.

DOI: 10.1103/PhysRevB.80.144107 PACS number(s): 61.50.Ks, 61.05.F−

I. INTRODUCTION

Geometrical frustration, related to the specific topology of certain crystal structures, plays a crucial role in forming exotic magnetic ground states. Suppression of long-range magnetic order and development of short-range correlated phases such as spin ice, spin glass, and spin liquid is the main feature of strongly frustrated magnets.[1] In some cases, frustration is partially or entirely released by structural distortions and long-range magnetic order is established at finite temperature. A well-known structural topology causing the presence of geometrical frustration is the two-dimensional kagome lattice consisting of corner-sharing triangles. Compositions whose structural motif embraces kagome layers are of great interest as model systems and have been the focus of numerous studies. Among these systems, one can distinguish the recently reported family of complex cobalt oxides $RBaCo_4O_7$ (R=rare-earth ion or Y).[2,3] Its crystal structure is built-up of alternating kagome and triangular cobalt lattices as shown in Fig. 1. The stacking of the triangular layers is the *AAA* type which makes this topology to be different from the well-known pyrochlore one where the *ABC* alternation takes place. The undistorted (parent) structure has hexagonal $P6_3mc$ symmetry and is an example of a so-called "framework" crystal structure formed by corner-sharing CoO_4 tetrahedra: the R and Ba cations occupy octahedral and cuboctahedral cavities, respectively, within the three-dimensional tetrahedral network. Cobalt ions are present in two charge states, Co^{3+} and Co^{2+}, respectively, in the ratio of 1:3. The ratio of the crystallographic sites in the triangular Co1($2a$) and kagome Co2($6c$) lattices is the same, so some degree of charge disproportionation between these positions may be expected below some critical temperature.[4–6]

This hexagonal structure was originally proposed for Ho-[2] and Y-based[3] compositions. However, a more recent structural study of $YbBaCo_4O_7$ revealed that the real symmetry for oxygen stoichiometric samples at room temperature is in fact trigonal, space group $P31c$.[7] Moreover, a temperature induced first-order structural phase transition, accompanied by anomalies in the magnetic and electrical properties, has been observed at $T_S \sim 175$ K. Similar transitions have been found in other members of the family with different R cations.[4,8–11] The critical temperature of the phase transition was shown to depend on R and varies from ~310 K for $R=Y$ (Ref. 8) down to ~165 K for R=Lu.[4,8] Orthorhombic symmetry has been proposed for the low-temperature phase by different authors but with various space groups namely $Cmc2_1$,[4] $Pmc2_1$,[12] and $Pbn2_1$ ($Pna2_1$ in standard setting).[7,13] The nature of the phase transition was also discussed on the

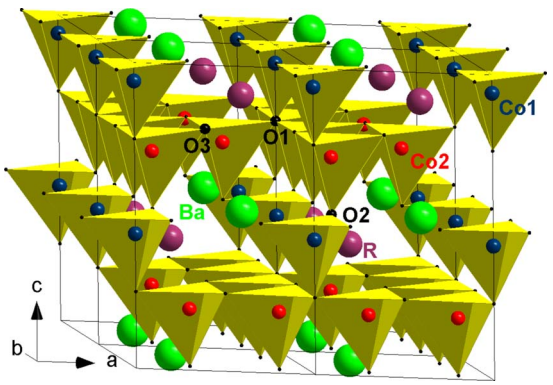

FIG. 1. (Color online) Polyhedral representation of the $P6_3mc$ hexagonal structure of $RBaCo_4O_7$ compounds. In the ideal structure with perfect tetrahedra, the unit cell parameters are related as $c_h=2\sqrt{\frac{2}{3}}a_h$ and the highly symmetric atomic positions are: R-$2b$(1/3,2/3,3/8), Ba-$2b$(2/3,1/3,1/2), Co1-$2a$(0,0,7/16), Co2-$6c$(1/6,−1/6,11/16), O1-$2a$(0,0,1/4), O2-$6c$(1/6,−1/6,1/2), and O3-$6c$(1/2,1/2,1/4). Cobalt ions in the triangular and kagome layers are denoted as Co1 (blue) and Co2 (red), respectively.

basis of different mechanisms. Huq *et al.*[7] concluded that the phase transition is of displacive type and that the driving force for the symmetry lowering is the presence of underbonded Ba^{2+} cations. Maignan *et al.*[14] argue for a magnetic origin via magnetostrictive effects and Nakayama *et al.*[4] suggested a charge ordering of Co^{2+} and Co^{3+} ions in the kagome and triangular lattice, respectively.

Gaining insight into the mechanism of the structural phase transition, through analysis of reliable structural information, is necessary in order to understand the magnetic properties of this class of materials. In particular, one needs to evaluate how the geometrical frustration is lifted by the symmetry lowering. Here, we present a study of $TmBaCo_4O_7$ by powder neutron diffraction, where crystallographic parameters are derived as a function of temperature. As for other members of the series,[7,13] we confirm the symmetry changes from trigonal $P31c$ to orthorhombic $Pna2_1$ at $T_S \sim 240$ K and show that the phase transition relates to complex rotations of the CoO_4 tetrahedra in both kagome and triangular sublattices, which are analyzed using symmetry consideration. The analysis and classification of the distortions in both trigonal and orthorhombic phases has been done in terms of basis functions of irreducible representations (irreps) of the $P6_3mc$ hexagonal space group. This symmetry is not observed experimentally, but a description based on a "virtual" $P6_3mc$ for which both $P31c$ and $Pna2_1$ space groups are isotropy subgroups, conveniently allows to classify the different modes involved. The main feature of these low-symmetry phases is that they involve substantial distortions of the CoO_4 tetrahedra. Our study reveals that the specific topology of the $RBaCo_4O_7$ crystal structure does not allow rotation of the tetrahedra as rigid units, a very uncommon fact for tetrahedral framework crystal structures. The presence of distortions, whatever the combination of rotational modes, has a clear analogy with magnetic frustrations in a "pseudospin space" where axial vectors (pseudospins), representing rotations of tetrahedral units, are coupled by effective antiferromagnetic exchange interactions.

II. STRUCTURE TOPOLOGY AND DISPLACIVE PHASE TRANSITIONS

Displacive phase transitions are widely spread in framework crystal structures.[15–19] They play an important role in determining physical properties of many compounds of special interest for solid state physics, chemistry and mineralogy. In particular, it has been shown that most phase transitions involve relative rotations of the polyhedral units in the lattice considered as rigid, i.e., without or with very little intraunit distortions.[20] It follows from the fact that forces within polyhedra are usually much stronger than the forces that act between them. Based on this observation Giddy *et al.*[16] and Dove *et al.*[17–19] have developed a specific theory within the context of the so-called rigid unit mode (RUM) model. The central point is that there exist vibrational modes that can propagate throughout the crystal lattice without distortion of polyhedra. The phonons associated with these RUMs have very low energy and can act as soft modes for displacive phase transitions. The well-studied and classified

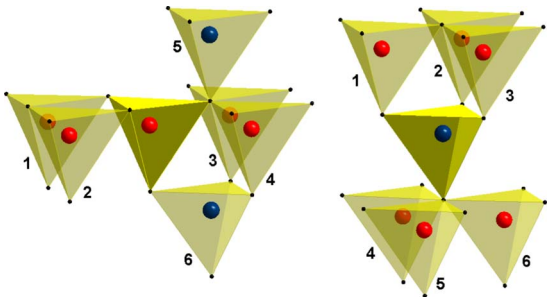

FIG. 2. (Color online) Six neighbor CoO_4 tetrahedra (light) corner-shared with an arbitrary chosen polyhedron (dark) in kagome (left) and triangular (right) layers.

octahedral tilt patterns in perovskites[21–24] are examples of condensation of this kind of phonons. A simple analysis based on the Maxwell theorem[25] can be used to estimate the "flexibility" of a crystal structure and conclude whether RUMs are geometrically allowed or not for a given topology.[16,18,26] Any structure with F degrees of freedom and C independent constraints will only be "floppy" if $F > C$. For any rigid polyhedron, $F=6$ (three translational and three rotational degrees of freedom). If two polyhedra are interconnected, there appear three constraints which are common for both polyhedra. In corner-sharing tetrahedral structures such as some spinels or most aluminosilicate minerals, each tetrahedron is connected to four other tetrahedra, i.e., $F=C$. The number of rigid unit modes is therefore $F-C=0$. However, as discussed by Dove *et al.*[17–19] and Giddy *et al.*,[16] symmetry often introduces degeneracy in the structure, making some of the constraints dependent. As a result, one would often find a few RUMs with wave vectors at special points or lines in reciprocal space, even in this case.

The situation for the $RBaCo_4O_7$ compounds is rather different. In the hexagonal structure ($P6_3mc$) proposed initially, each tetrahedron is connected to six neighbor tetrahedra (Fig. 2) and hence $F-C=-3$ which means that the structure is strongly overconstrained and no RUMs are expected in the phonon spectrum.[26] In other words, there are no easy ways to distort the structure (with rigid modes) and this fact brings additional interest to investigate thoroughly the phase transitions in these materials. In particular, it is interesting to determine if the lack of RUM is related to the presence of geometrical frustration. To discuss it, one should recall that rotations of metal coordination units (polyhedra) can be represented as axial vectors on the metal positions (Fig. 3). The directions of the pseudovectors coincide with directions of the rotational axes and their magnitudes are proportional to the angle of the rotation. A condensation of a particular RUM phonon can be considered as the establishment of long-range ordering of the corresponding axial vectors. The situation is similar to long-range magnetic order, where the connection between adjacent polyhedra via shared vertices is a direct analogy to magnetic exchange interactions.

Let consider now rotations of the rigid tetrahedra in the kagome layer of the $P6_3mc$ structure about the $[16,8,3]$, $[\bar{8},8,3]$ and $[\bar{8},1\bar{6},3]$ crystallographic axes shown in Fig. 3. As it will be demonstrated below, rotations about these axes are a part of structural distortions which take place in

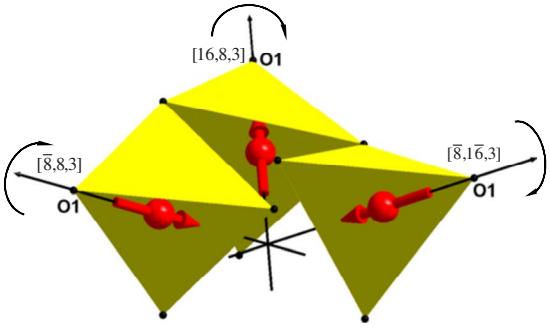

FIG. 3. (Color online) Structural fragment of a kagome layer, representing rotations of rigid CoO_4 tetrahedra about the [16,8,3], [$\bar{8}$,8,3], and [$\bar{8}$,1$\bar{6}$,3] crystallographic axes passing through the cobalt and O1 oxygen ions. (Note that the terahedra can rotate as rigid units only if two of them are decoupled. A rotation of the coupled tetrahedra results in their inevitable distortions.)

$TmBaCo_4O_7$ at low temperatures. The axial vectors coincide with the positive directions of the axes if an anticlockwise rotation takes place. A rotation of any tetrahedron requires rotation of the two adjacent ones about their (individual) axes by the same angle but in opposite directions, so that it is impossible to keep the latter polyhedra linked without distorting them. One can say that there are effective "antiferromagnetic interactions" between these axial vectors which cannot be simultaneously satisfied and the distortions of the tetrahedra play the same role as frustrations in a real magnetic system. From this point of view, displacive phase transitions in this kind of structures are similar to magnetic ordering in magnetically frustrated systems.

III. EXPERIMENTAL

The sample of $TmBaCo_4O_{7+\delta}$ was prepared by a standard ceramic technique from high-purity Tm_2O_3, $BaCO_3$, and Co_3O_4, with a final firing at 1150 °C in air followed by furnace cooling. The as-made sample was treated in a nitrogen atmosphere to obtain a sample with $\delta \sim -0.05(5)$ as determined by reduction in a 5% H_2/Ar mixture on a Perkin-Elmer TGA-7.

Neutron diffraction data were collected on the general materials diffractometer (GEM), at the ISIS facility, Rutherford Appleton Laboratory (U.K.). A 2 g sample was enclosed in a cylindrical vanadium can, placed in a close cycle refrigerator. Data were collected on warming between 10 and 260 K in steps of 10 K. Rietveld refinements were carried out with the program FullProf.[27]

IV. RESULT AND DISCUSSION

A. Crystal structure at $T=260$ K

The neutron diffraction patterns of $TmBaCo_4O_7$ at T =260 K can be indexed with the hexagonal unit cell [a_h =6.2754(1) Å, c_h=10.2404(1) Å]. The reflection conditions (hhl; $l=2n$ and $00l$; $l=2n$) are consistent with the $P6_3mc$ space group originally proposed for Ho[2] and Y-based[3] analogs. However, the refinement of the crystal structure with this symmetry is rather poor. Unphysically large thermal parameters for the O2 and O3 oxygen positions and poor fitting of reflections at large scattering vector ($\boldsymbol{Q}$) point to a less symmetric distribution of the oxygen in the unit cell. To account for this, the isotropy subgroups of $P6_3mc$, keeping the same translational invariance, were analyzed.[28–30] Three maximal subgroups, namely, $P6_3$, $P3m1$, and $P31c$ related to the center of the Brillouin zone (modulation vector $\boldsymbol{k}=0$) preserve the metric of the unit cell (Table I). The first two subgroups are not compatible with the observed reflection conditions, whereas the third one, has the same conditions as hexagonal $P6_3mc$. Taking into account this fact as well as the results of Huq *et al.*,[7] a model in the $P31c$ space group was tested in the refinement, resulting in a much better agreement with the experimental data [Fig. 4(a)]. The refined structural parameters are summarized in Table II. The $P31c$ space group is an isotropy subgroup of $P6_3mc$ associated with the one-dimensional Γ_3 irreducible representation (Miller-Love notation).[31] This group-subgroup relation allows to consider the trigonal structure of $TmBaCo_4O_7$ as a distorted variant of an "ideal" crystal structure with the hexagonal symmetry, which probably can be stable at higher temperatures. To clarify the driving force and mechanism of the symmetry

TABLE I. Isotropy subgroup, irreducible representation, direction of order parameter in the representation space, origin and lattice vectors of the subgroup in respect of the basis of the parent $P6_3mc$ space group.

Subgroup	Irrep	Order param.	Lattice vectors	Origin
$P6_3$(#173)	Γ_2	(a)	(1,0,0)(0,1,0)(0,0,1)	(0,0,0)
$P31c$(#159)	Γ_3	(a)	(1,0,0)(0,1,0)(0,0,1)	(0,0,0)
$P3m1$(#156)	Γ_4	(a)	(1,0,0)(0,1,0)(0,0,1)	(0,0,0)
$Cmc21$(#36)	Γ_5	(a,0)	(0,−1,0)(2,1,0)(0,0,1)	(0,0,0)
Cm(#8)	Γ_6	(a,0)	(2,1,0)(0,−1,0)(0,0,−1)	(0,0,0)
Cc(#9)	Γ_6	(0,a)	(0,−1,0)(2,1,0)(0,0,1)	(0,0,0)
$Pmc2_1$(#26)	M_1	(a,0,0)	(0,−1,0)(2,1,0)(0,0,1)	(0,0,0)
$Pna2_1$(#33)	M_2	(a,0,0)	(2,1,0)(0,1,0)(0,0,1)	(0,0,0)
$Pca2_1$(#29)	M_3	(a,0,0)	(2,1,0)(0,1,0)(0,0,1)	(1/2,0,0)
$Pmn2_1$(#31)	M_4	(a,0,0)	(0,−1,0)(2,1,0)(0,0,1)	(1/2,1/4,0)

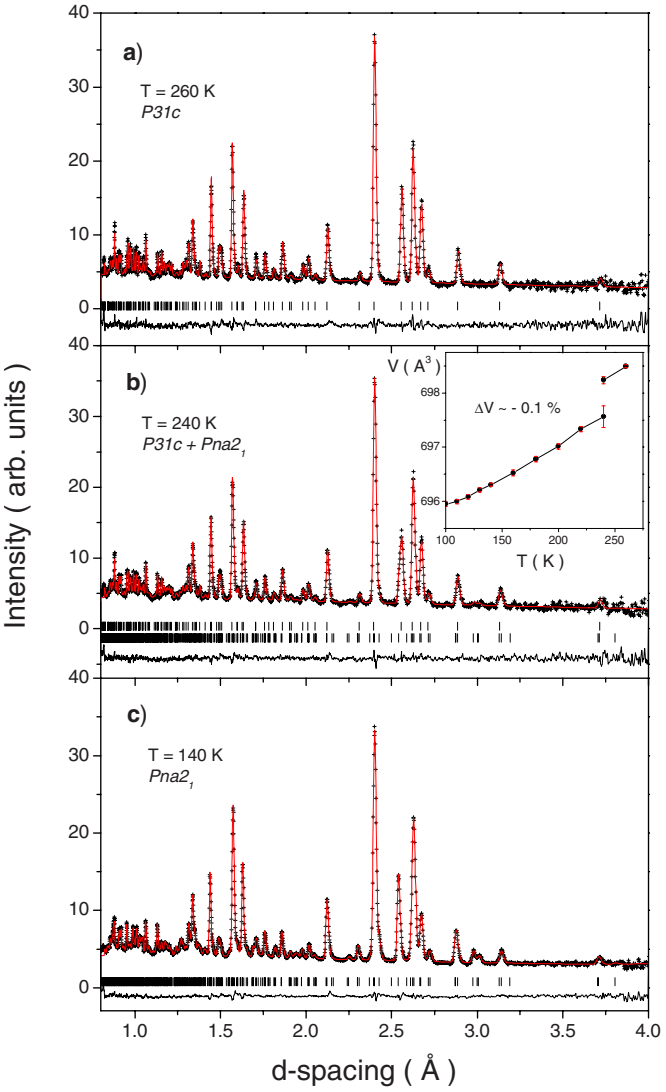

FIG. 4. (Color online) Rietveld refinements of neutron powder diffraction patterns obtained at different temperatures as a function of d spacing. The cross symbols and (red) solid line represent the experimental and calculated intensities, respectively, and the line below is the difference between them. Tick marks indicate the positions of Bragg peaks according to the respective space groups. The inset shows temperature variation of unit cell volume in a vicinity of the phase transition.

lowering, a mode decomposition of the distorted structure (trigonal) in terms of symmetry-adapted atomic displacements of the $P6_3mc$ structure has been performed. The analysis was done with the help of *ISODISPLACE*,[32] starting with all atoms in the parent structure in their highly symmetric positions. Moreover, atomic components, $\varphi^{k_L\nu}_{i,\alpha,\lambda}(\boldsymbol{r}_i)$, of pseudovector basis functions, $\boldsymbol{\psi}^{\nu}_{\lambda}(\boldsymbol{r}_i+\boldsymbol{t}_n)$, of the Γ_3 irrep, on the cobalt positions, $\boldsymbol{r}_i+\boldsymbol{t}_n$, were calculated too (see Appendix for details) and compared with the result of the mode decomposition. This allowed us to correlate the atomic displacements with some of the rotational modes (Table III) which in this case are more convenient to represent the structural distortions.

The decomposition revealed that the mode $\Gamma_3[\mathrm{O2}:c]A''(a)$,[33] related to displacement of some oxygen ions (O2 in the parent structure) lying in the same ab plane as barium, has the largest amplitude $\sim -0.308(4)$ Å [Fig. 5(a)]. This distortion mode can be clearly related to a rotation of the $\mathrm{Co}(1)\mathrm{O}_4$ tetrahedra of the triangular lattice around the hexagonal axis of the parent structure. The corresponding symmetrized axial components on the $2a$ cobalt position ($\varphi_{i,\alpha,\lambda=1}$ in Table III) are shown in Fig. 5(a). The mode amplitude, which is three to five times bigger than the amplitudes of any others modes with the Γ_3 symmetry, unambiguously points to the primary character of this type of distortion. A rotation of corner-sharing polyhedra is a common mechanism of displacive phase transitions in many framework crystal structures. The well-known examples are aluminosilicate minerals containing linked SiO_4 and AlO_4 tetrahedra[18] as well as perovskitelike compounds with three-dimensional octahedral networks.[34] In most cases, the driving force for the symmetry lowering is bonding requirements for some of the atoms located in cavities at the interstices of the polyhedral network. To verify this possibility for $TmBaCo_4O_7$, the bond valence sum (BVS) calculations have been carried out both with and without the presence of the Γ_3 distortion modes. In order to "switch off" the atomic displacements involved in the symmetry lowering to trigonal $P31c$, the amplitudes of all distortion modes related to the Γ_3 irreducible representation were fixed to zero and new atomic coordinates were generated by *ISODISPLACE*. As found by Huq *et al.*[7] in the case of $YbBaCo_4O_7$ in the $P31c$ phase, Ba^{2+} cations are strongly underbonded in the hypothetical $P6_3mc$ phase of $TmBaCo_4O_7$. In the hexagonal phase, the BVS of Ba^{2+} is very small, ~ 1.20, but is significantly increased (1.42) in the trigonal space group. The symmetry change also improves the bond valence requirement for Tm^{3+} cations, which oppositely to barium, are essentially overbonded (BVS ~ 3.50 in the $P6_3mc$ and 3.36 in the $P31c$ phases). One should point out that there are no order-disorder modes with the Γ_3 symmetry, which means that any type of ordering, including charge ordering, between Co^{3+} and Co^{2+} cannot be the primary order parameter of the $P6_3mc \rightarrow P31c$ phase transformation.

The rotation of tetrahedra in the triangular layers, already discussed, is an effective way to adjust the bond valence requirements of Ba^{2+}, because it involves shifts of coplanar O2 ions directly toward barium cations [Fig. 5(a)]. In addition, this results in an increase in the Tm-O(2) distances,

TABLE II. Structural parameters of $TmBaCo_4O_7$ at T=260 K. Space group $P31c$, unit cell parameters: a_h=6.2754(1) Å and c_h =10.2404(3) Å, reliability factors: R_p=3.65% and R_{wp}=4.34%.

Atom (Wyckoff)	x	y	z	B_{iso} (Å^2)
Tm($2b$)	2/3	1/3	0.881(1)	0.7(1)
Ba($2b$)	2/3	1/3	0.5	1.0(2)
Co1($2a$)	0	0	0.440(2)	0.2(2)
Co2($6c$)	0.158(2)	0.821(2)	0.688(2)	0.9(1)
O1($2a$)	0	0	0.251(2)	0.32(2)
O2($6c$)	0.118(1)	0.784(1)	0.500(1)	0.87(1)
O3($6c$)	0.516(1)	0.515(1)	0.755(2)	2.0(1)

TABLE III. Atomic components, $\varphi^{k_L\nu}_{i,\alpha,\lambda}(\boldsymbol{r}_i)$, of pseudovector basis functions, $\boldsymbol{\psi}^{\nu}_{\lambda}(\boldsymbol{r}_i+\boldsymbol{t}_n)$, of $\nu=\Gamma_3$ irreducible representation of $\boldsymbol{k}=0$ wave-vector group for triangular $2a$ and kagome $6c$ sublattices.

	Wyckoff c, $i=1\ldots6$						Wyckoff a, $i=1,2$	
$\varphi_{i,\alpha,\lambda}$	$x,-x,z$ [a]	$2x,x,z+1/2$	$x,2x,z$	$-x,x,z+1/2$	$-2x,-x,z$	$-x,-2x,z+1/2$	$0,0,z$ [b]	$0,0,z+1/2$
$\varphi_{i,x,1}$	$\frac{1}{\sqrt{3}}$	$-\frac{2}{\sqrt{3}}$	$\frac{1}{\sqrt{3}}$	$\frac{1}{\sqrt{3}}$	$-\frac{2}{\sqrt{3}}$	$\frac{1}{\sqrt{3}}$	0	0
$\varphi_{i,y,1}$	$-\frac{1}{\sqrt{3}}$	$-\frac{1}{\sqrt{3}}$	$\frac{2}{\sqrt{3}}$	$-\frac{1}{\sqrt{3}}$	$-\frac{1}{\sqrt{3}}$	$\frac{2}{\sqrt{3}}$	0	0
$\varphi_{i,z,1}$	0	0	0	0	0	0	1	−1
$\varphi_{i,x,2}$	0	0	0	0	0	0		
$\varphi_{i,y,2}$	0	0	0	0	0	0		
$\varphi_{i,z,2}$	1	−1	1	−1	1	−1		

[a] $x\sim1/6$, $z\sim11/16$.
[b] $z\sim7/16$.

optimizing anion environment for Tm^{3+} cations. However, displacement of only O2 ions is definitely not sufficient to satisfy completely the bonding conditions. Moreover, the amplitude of these rotations is limited by the associated distortions of tetrahedra in the kagome sublattice. One way to quantify polyhedral distortions is to define the parameter Δ, as: $\Delta=\sqrt{\frac{\Sigma[\langle\text{Co-O}\rangle-(\text{Co-O})]^2}{\langle\text{Co-O}\rangle^2}}$, where $\langle$Co-O$\rangle$ is the average Co-O bond length, and the summation is done over the four Co-O bonds. In the trigonal structure, this parameter equals $\sim$0.001 for the triangular $Co(1)O_4$ tetrahedra and it is twenty times larger $\sim$0.002 for the kagome $Co(2)O_4$ ones. The interconnection of the triangular and kagome sublattices via the common O2 oxygen makes the latter to react to the polyhedral tilting but the absence of RUMs in the structure does not allow the kagome sublattice to adopt some displacive modes keeping the $Co(2)O_4$ tetrahedra undistorted.

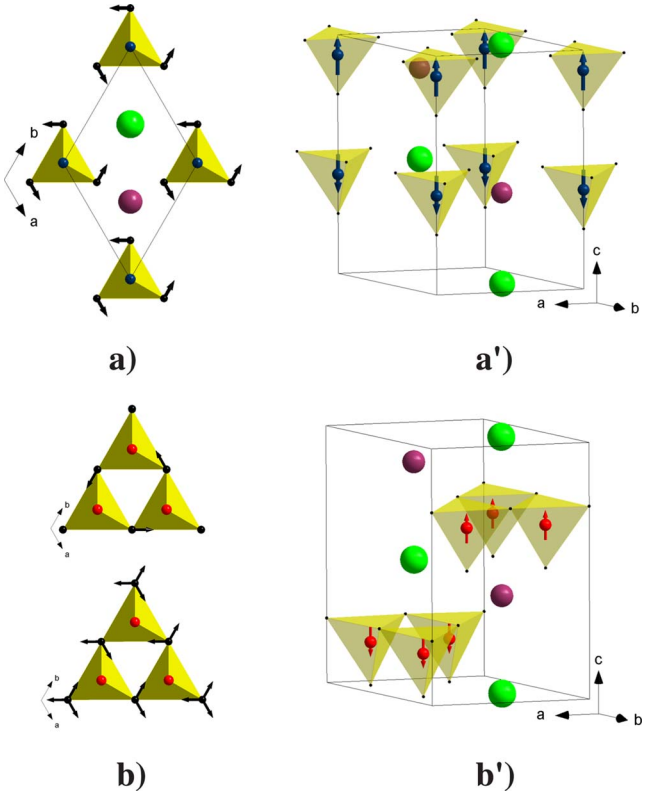

FIG. 5. (Color online) Oxygen displacements in the $\Gamma_3[\text{O2}:c]A''(a)$ (a) and $\Gamma_3[\text{O3}:c]A''(a)$ (b) distortion-modes. (a′) and (b′)—their corresponding pseudovector representations.

The mode decomposition analysis revealed also shifts of the O3 parent ions. The corresponding $\Gamma_3[\text{O3}:c]A''(a)$ displacive mode is shown in Fig. 5(b) (upper scheme). The amplitude of these displacements is three and half times smaller [$\sim$0.087(6) Å] than the amplitude of the oxygen displacements in the $\Gamma_3[\text{O2}:c]A''(a)$ mode. The shift of the O3 ions affects only weakly the bonding conditions of barium and thulium and can be considered as a response of the kagome layers to the tetrahedral tilting in the triangular lattice. In other words, this shift helps to minimize the elastic energy related to the distortions of the polyhedra in the kagome layers. Using the pseudovector formalism (axial components $\varphi_{i,\alpha,\lambda=2}$ in Table III), the $\Gamma_3[\text{O3}:c]A''(a)$ displacive mode can be presented as ferrodistorsive rotations of tetrahedra within the kagome sublattice about the c axis [Fig. 5(b) bottom scheme and Fig. 5(b′)]. One can say that the primary rotations of the tetrahedra in the triangular lattice induce ferrodistorsive rotations of the polyhedra in the kagome layers. Thus, in spite of the Γ_3 symmetry, this type of distortions does not energetically drive the phase transition and, in this respect, cannot be classified as a primary order parameter. Figure 6 shows the summarized pseudovector representation of the main distortions of both the triangular and kagome sublattices in the trigonal $P31c$ phase.

Apparently, the presence of the single $\Gamma_3[\text{O2}:c]A''(a)$ primary rotational mode which allows displacement of only a fraction of the oxygen ions ($\sim$43% of the total oxygen sites), restricts the ability of the lattice in the trigonal $P31c$ phase to improve the bonding conditions of Ba^{2+} and Tm^{3+} cations.

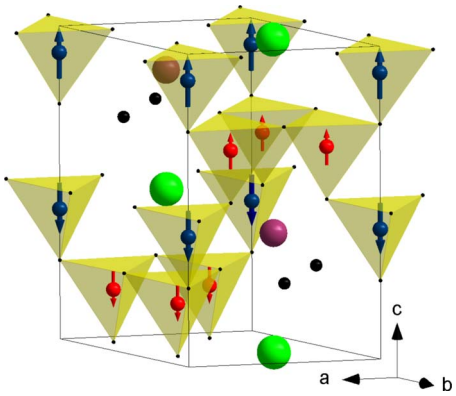

FIG. 6. (Color online) Axial vectors on cobalt positions representing tetrahedral tilting for both the triangular and kagome sublattices in the trigonal $P31c$ phase.

This can be the reason of the structure instability and further symmetry lowering at $T_S \sim 240$ K. From this point of view, it is quite logical to assume that the primary modes in the low-temperature phase induce displacements of more oxygen. At the same time, it should be pointed out that oxygen ions in the O1 parent position shared by four neighbor tetrahedra are of special points of the structure. Their shift is energetically very unfavorable because it involves distortions of the four tetrahedral units simultaneously.

B. Low-temperature crystal structure

The diffraction patterns obtained at $T \leq 220$ K indicate splitting of some of the fundamental Bragg peaks as well as the presence of weak superstructure reflections. In order to account for all the observed reflections, the minimal cell is an orthorhombic $\sqrt{3}a_h \times a_h \times c_h$ supercell. The phase transition, occurring between 260 and 220 K has a pronounced first-order character which is evidenced by a phase coexistence at T=240 K [Fig. 4(b)] and clear discontinuity in thermal variation of the unit cell volume [Fig. 4(b) inset]. As pointed out in the introduction, there is no consensus in the literature about the symmetry of the low-temperature phase. To systematically approach the problem, all isotropy subgroups[28–30] of the $P6_3mc$ space group, associated with $\boldsymbol{k}$ points of high symmetry, have been considered in turn. The subgroups which are consistent with the observed breakdown of translational symmetry are listed in Table I, along with their corresponding representations, order parameters, and lattice vectors with respect to the basis of the parent group. While orthorhombic symmetry successfully indexes all peaks, subgroups of lower symmetry, in particular monoclinic, were included too, because effects of pseudosymmetry and the limited experimental resolution can result in underestimation of the singony. The observation of the reflections $(0kl;k,l=2n+1)/(h0l;h,l=2n+1)$ in the $\sqrt{3}a_h \times a_h \times c_h / a_h \times \sqrt{3}a_h \times c_h$ supercell indexation are consistent only with two subgroups, $Pna2_1$ and $Pmn2_1$ from Table I. At the same time, the systematic absence of the reflections $(h0l;h=2n+1)/(0kl;k=2n+1)$ points to the presence of the glide plane with $a/2/b/2$ translational component. The latter observation makes the $Pna2_1$ space group the most probable.

In addition to the symmetry compatibility with reflection conditions, some additional criteria related to the symmetry analysis of the high-temperature phase can be applied. In particular, the low-temperature symmetry should allow rotations of the tetrahedra in the triangular layers about the c axis, as observed in the high-temperature trigonal structure $P31c$. The presence of this rotational mode below T_S is expected because it is a very efficient way to improve the barium and thulium bonding conditions, as discussed above, and it is the only type of polyhedral tilting in the triangular sublattice which does not involve displacements of the O1 parent ions (these displacements, are energetically very expensive). This criterion sets essential restrictions on the low-temperature symmetry. From a group-theoretical point of view, it means that the irrep ν, which mediates the symmetry lowering, should satisfy the following conditions.

(i) The irrep subduction frequency, m_ν, in the pseudovector reducible representation on the Co1($2a$) position must not equal zero:

$$m_\nu = \frac{1}{n(g)} \sum_g \chi(g)\chi^{*\nu}(g) \neq 0,$$

where $n(g)$ is the number of elements in $P6_3mc$, $\chi(g)$, and $\chi^\nu(g)$ are characters of the element, g, in the reducible and irreducible representations, respectively. The sum is taken over all symmetry elements of the $P6_3mc$ group.

(ii) Symmetrized combinations of the z components of axial vectors on the Co1($2a$) position should transform as basis functions, $\boldsymbol{\psi}^\nu_\lambda(\boldsymbol{r}_i+\boldsymbol{t}_n)$, of this irrep:

$$T(g)\boldsymbol{\psi}^\nu_\lambda = \sum_{j=1}^{d^\nu} \boldsymbol{\psi}^\nu_j D^\nu_{j\lambda}(g),$$

$$\boldsymbol{\psi}^\nu_\lambda(\boldsymbol{r}_i+\boldsymbol{t}_n) = \sum_L^{l_k} \sum\nolimits^{\oplus}_{n=1\ldots N} \left[\sum\nolimits^{\oplus}_{i=1\ldots\sigma,\alpha=x,y,z} C^{\boldsymbol{k}_L\nu}_\lambda \varphi^{\boldsymbol{k}_L\nu}_{i,\alpha,\lambda} \{\boldsymbol{e}_{i\alpha}\} \right] \times \exp(i\boldsymbol{k}_L\boldsymbol{t}_n); \quad \varphi^{\boldsymbol{k}_L\nu}_{i,x,\lambda}, \varphi^{\boldsymbol{k}_L\nu}_{i,y,\lambda} = 0, \varphi^{\boldsymbol{k}_L\nu}_{i,z,\lambda} \neq 0,$$

where $T(g)$ is an operator acting in the representation space, $D^\nu_{j\lambda}(g)$ is d^ν-dimensional matrix onto which the irrep ν maps element g.

A relevant analysis showed that both conditions are satisfied only by two irreps: M_2 and M_3. Thus, the allowed subgroups are $Pna2_1$ and $Pca2_1$. These subgroups, along with $Pmn2_1$, were tested in the refinement. As expected, the $Pna2_1$ gives much better agreement with the experiment. The quality of the fit is excellent; this fact in combination with the analysis of the reflections condition and additional symmetry arguments considered above leaves no doubts about the correct choice of symmetry [Fig. 4(c)]. Using the structural parameters refined in the $Pna2_1$ space group (Table IV), BVS calculations were performed. The result showed that the symmetry lowering results in an additional improvement of the bonding conditions for both Ba^{2+} (BVS $\sim$ 1.58) and Tm^{3+} (BVS $\sim$ 3.24) cations in comparison with the trigonal structure. Thus, our results for the structural

TABLE IV. Structural parameters of $TmBaCo_4O_7$ at T=140 K. Space group $Pna2_1$, unit cell parameters: a=10.9176(3), b=6.2739(2) Å, and c=10.1658(2) Å, reliability factors: R_p=2.03% and R_{wp}=2.41%.

Atom (Wyckoff)	x	y	z	B_{iso} (Å^2)
Tm(4a)	0.670(1)	−0.004(1)	0.8836(6)	0.42(5)
Ba(4a)	2/3	0	0.5	0.77(8)
Co1(4a)	−0.003(3)	0.000(3)	0.940(1)	0.6(2)
Co21(4a)	0.172(2)	0.006(4)	0.684(2)	0.46(7)
Co22(4a)	0.088(2)	−0.257(4)	0.191(2)	0.46(7)
Co23(4a)	0.921(2)	−0.258(4)	0.688(2)	0.46(7)
O1(4a)	−0.002(2)	0.001(6)	0.251(1)	0.37(7)
O21(4a)	0.1614(7)	0.049(1)	0.497(2)	0.77(5)
O22(4a)	0.0993(6)	−0.231(1)	−0.001(2)	0.77(5)
O23(4a)	0.9401(6)	−0.268(1)	0.496(2)	0.77(5)
O31(4a)	0.493(1)	−0.002(4)	0.247(1)	0.87(6)
O32(4a)	0.256(1)	0.225(2)	0.782(1)	0.87(6)
O33(4a)	0.752(1)	0.220(2)	0.221(1)	0.87(6)

behavior of $TmBaCo_4O_7$ are entirely consistent with those reported by Huq *et al.*[7] for $YbBaCo_4O_7$ pointing to their common character.

To clarify the main distortions driving the first-order phase transition, a mode decomposition of the orthorhombic phase with respect to the symmetry-adapted atomic displacements of the parent hexagonal structure has been performed. Four primary modes, $M_2[O2:c]A_2''(a)$, $M_2[O2:c]A_1''(a)$, $M_2[O3:c]A_2'(a)$, and $M_2[O3:c]A_1'(a)$ having the largest amplitudes, 0.307(8) Å, 0.245(5) Å, −0.313(8) Å, and 0.172(9) Å, respectively, and involving displacements of the oxygen ions from both the O2 and O3 parent positions, as it is shown in Fig. 7, drive the phase transition. Displacements of the oxygen ions from the O1 parent position were found to be absent in this phase. As mentioned above, any displacements of these ions should involve distortions of four tetrahedral units simultaneously, making these displacements energetically very expensive. To complete the results of the decomposition analysis and assign the obtained atomic displacements to rotational modes, atomic components of pseudovector basis functions of the M_2 irrep for both Co1(2a) and Co2(6c) positions were calculated too. It should be pointed out that $Pna2_1$ space group is an isotropy subgroup of $P6_3mc$ related to one arm of the three-arm wave-vector star ($\boldsymbol{k}_1=\boldsymbol{a}^*/2$, $\boldsymbol{k}_2=\boldsymbol{b}^*/2$, and $\boldsymbol{k}_3=-\boldsymbol{a}^*/2+\boldsymbol{b}^*/2$) associated with the M reciprocal point. For our analysis, only the basis functions for the first representative arm, $\boldsymbol{k}_1=\boldsymbol{a}^*/2$, need to be calculated. The corresponding little group is the orthorhombic group $Cmc2_1$ which splits the 6c parent position of cobalt ions in the kagome sublattice into two orbits; orbit 1 and orbit 2 with multiplicity four and two, respectively. The 2a position of the cobalt in the triangular lattice remains unsplit. Results of the calculations for all the orbits in the primary hexagonal unit cell are presented in Table V. The atomic components in any unit cell related with the primary one via translation $\boldsymbol{t}_n$ can be obtained by the expression:

$$\varphi_{i,\alpha,\lambda}(\boldsymbol{r}_i+\boldsymbol{t}_n)=\varphi_{i,\alpha,\lambda}(\boldsymbol{r}_i)\exp(i\boldsymbol{k}_1\boldsymbol{t}_n).$$

A combination of the $M_2[O2:c]A_2''(a)$ and the $M_2[O2:c]A_1''(a)$ distortions represents rotations of tetrahedra

TABLE V. Atomic components, $\varphi_{i,\alpha,\lambda}^{k_L\nu}(\boldsymbol{r}_i)$, of pseudovector basis functions, $\boldsymbol{\psi}_\lambda^\nu(\boldsymbol{r}_i+\boldsymbol{t}_n)$, of $\nu=M_2$ irreducible representation of $\boldsymbol{k}_1=\boldsymbol{a}^*/2$ wave vector group for triangular 2a and kagome 6c sublattices.

	Wyckoff c							
	Orbit 1, i=1…4				Orbit 2, i=1,2		Wyckoff a, i=1,2	
$\varphi_{i,\alpha,\lambda}$	$x,-x,z$ [a]	$x,2x,z$	$-x,x,z+1/2$	$-x,-2x,z+1/2$	$2x,x,z+1/2$	$-2x,-x,z$	$0,0,z$ [b]	$0,0,z+1/2$
$\varphi_{i,x,1}$	1	1	−1	−1	$\frac{2}{\sqrt{3}}$	$-\frac{2}{\sqrt{3}}$	0	0
$\varphi_{i,y,1}$	1	0	−1	0	$\frac{1}{\sqrt{3}}$	$-\frac{1}{\sqrt{3}}$	0	0
$\varphi_{i,z,1}$	0	0	0	0	0	0	1	1
$\varphi_{i,x,2}$	$\frac{1}{\sqrt{3}}$	$\frac{1}{\sqrt{3}}$	$-\frac{1}{\sqrt{3}}$	$-\frac{1}{\sqrt{3}}$	0	0	$-\frac{2}{\sqrt{3}}$	$\frac{2}{\sqrt{3}}$
$\varphi_{i,y,2}$	$-\frac{1}{\sqrt{3}}$	$\frac{2}{\sqrt{3}}$	$\frac{1}{\sqrt{3}}$	$-\frac{2}{\sqrt{3}}$	0	0	$-\frac{1}{\sqrt{3}}$	$\frac{1}{\sqrt{3}}$
$\varphi_{i,z,2}$	0	0	0	0	1	1	0	0
$\varphi_{i,x,3}$	0	0	0	0				
$\varphi_{i,y,3}$	0	0	0	0				
$\varphi_{i,z,3}$	1	1	1	1				

[a] $x\sim 1/6$, $z\sim 11/16$.
[b] $z\sim 7/16$.

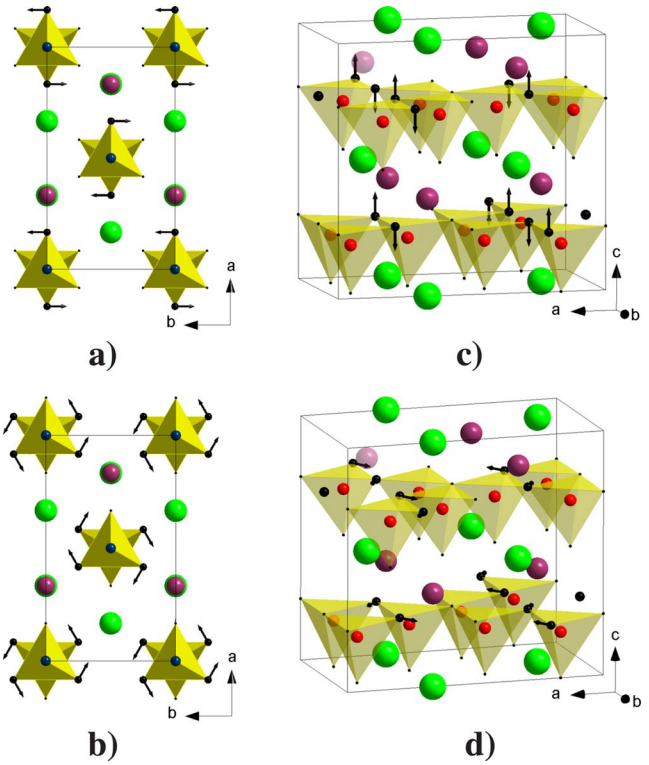

FIG. 7. (Color online) Oxygen displacements in the $M_2[O2:c]A_2''(a)$ (a), $M_2[O2:c]A_1''(a)$ (b), $M_2[O3:c]A_2'(a)$ (c), and $M_2[O3:c]A_1'(a)$ (d) primary distortion modes lowering the symmetry down to orthorhombic $Pna2_1$. The distortions are shown in the orthorhombic $\sqrt{3}a_h \times a_h \times c_h$ supercell.

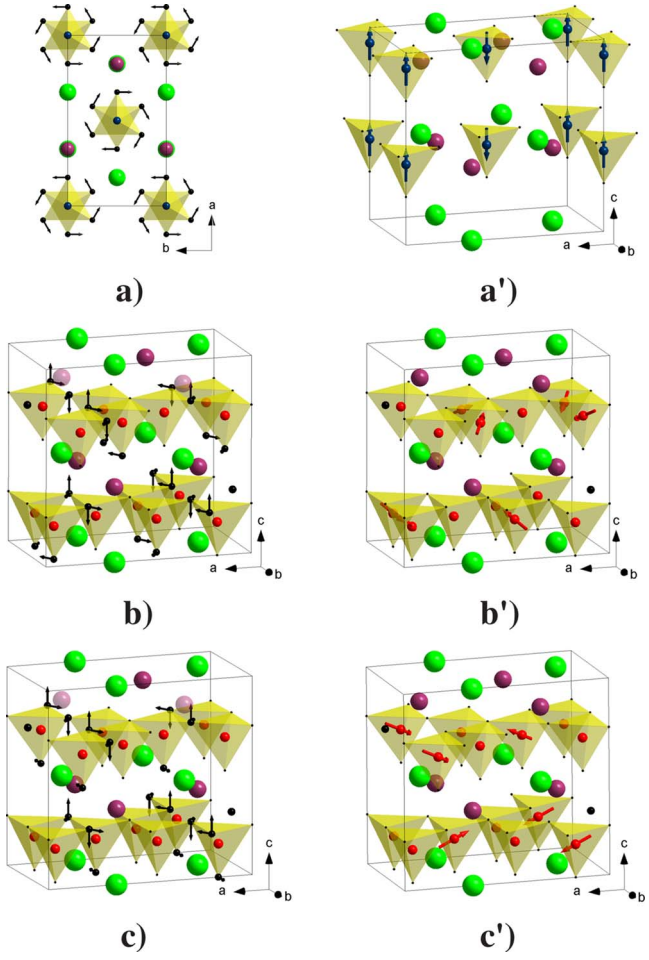

FIG. 8. (Color online) Combinations of the $M_2[O2:c]A_2''(a)$ $+M_2[O2:c]A_1''(a)$ (a), $M_2[O3:c]A_2'(a)+M_2[O3:c]A_1'(a)$ $+M_2[O2:c]A_1''(a)$ (b), and $M_2[O3:c]A_2'(a)+M_2[O3:c]A_1'(a)$ $+M_2[O2:c]A_2''(a)$ (c) displacive modes related to rotations of tetrahedral units coordinated around cobalt ions from different sublattices; (a′)—2*a* cobalt position in triangular layers, (b′)—orbit 1 and (c′)—orbit 2 of the 6*c* cobalt position in kagome layers. The distortions are shown in the orthorhombic $\sqrt{3}a_h \times a_h \times c_h$ supercell.

in triangular layers about the *c* axis, in agreement with the suggestions presented earlier. The oxygen displacements and the corresponding axial components for the Wyckoff position 2*a* ($\varphi_{i,\alpha,\lambda=1}$ in Table V) are shown in Figs. 8(a) and 8(a′), respectively. Superpositions of the $M_2[O3:c]A_2'(a)$ $+M_2[O3:c]A_1'(a)+M_2[O2:c]A_1''(a)$ and $M_2[O3:c]A_2'(a)$ $+M_2[O3:c]A_1'(a)+M_2[O2:c]A_2''(a)$ modes correspond to rotations of the tetrahedra in the kagome sublattice about the $[\bar{8},8,3]$, $[\bar{8},1\bar{6},3]$, $[8,\bar{8},3]$, [8,16,3], [16,8,3] and $[1\bar{6},\bar{8},3]$ crystallographic axes [Figs. 8(b) and 8(c)]. The former combination tilts tetrahedra coordinated around cobalt ions from the orbit 1, the latter—tetrahedra coordinated around cobalt ions from the orbit 2. The polyhedral units of the orbit 1 are tilted about the $[\bar{8},8,3]$ and $[\bar{8},1\bar{6},3]$ axes for the kagome layer with $z \sim 11/16$ and about the $[8,\bar{8},3]$ and [8,16,3] axes for the layer with $z \sim 3/16$. The coordinated units of the orbit 2 located in these layers are tilted about the [16,8,3] and $[1\bar{6},\bar{8},3]$ axes, respectively. In all cases, the rotational axes pass through the cobalt ions and the oxygen ions from the O1 parent position. Thus, for any polyhedral rotations, these oxygen ions are kept nondisplaced. The appropriate pseudovector description of the distortions for both orbits can be obtained by mixing the basic atomic components given in Table V as: $\sqrt{3}C_2'\varphi_{i,\alpha,\lambda=2}+\frac{3C_3'}{8}\varphi_{i,\alpha,\lambda=3}; C_2'=-C_3'$ [Fig. 8(b′)] and $\sqrt{3}C_1''\phi_{i,\alpha,\lambda=1}+\frac{3C_2''}{8}\phi_{i,\alpha,\lambda=2}; -C_1''=C_2''$ [Fig. 8(c′)], for the orbit 1 and the orbit 2, respectively. It should be pointed out that values of the axial vectors on the cobalt sites belonging to the same orbit are constrained by symmetry to be equal; therefore, the corresponding polyhedral units should rotate by equal angles. As a result, displacement components of some oxygen ions (O31 in Table IV) practically cancel each other and these ions remain very close to their highly symmetric positions. A total pseudovector representation of the rotational distortions in the orthorhombic $Pna2_1$ phase is shown in Fig. 9.

Let consider two structural fragments representing corner-linked tetrahedra from a kagome layer. In the first fragment, three polyhedra share one common oxygen ion (O1 parent position), in the second fragment there are three oxygen ions (O2 parent position) coupling adjacent polyhedra (Fig. 9). Each fragment contains two cobalt atoms from the orbit 1 and one atom from the orbit 2. In both cases, tetrahedra coordinated around cobalt ions from different orbits rotate by different angles. However, in the first fragment they are ro-

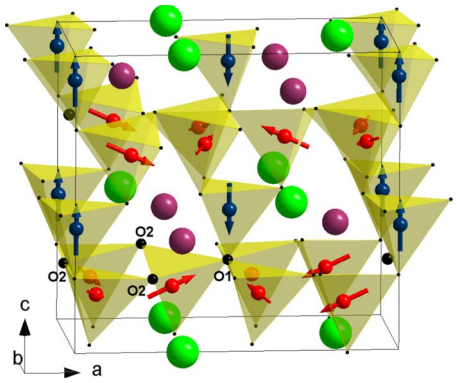

FIG. 9. (Color online) Axial vectors on the cobalt positions representing tetrahedral tilting for both kagome and triangular sublattices in the orthorombic $Pna2_1$ phase. In the kagome sublattice axial vectors on cobalt sites from the orbit 1 and orbit 2 are presented by the small and large arrows, respectively.

tated in the same (clockwise/anticlockwise) way about the relevant axes, whereas in the second fragment, polyhedral units from the orbit 1 and the orbit 2 rotate in opposite way. Distortions of the tetrahedra appear in the second structural fragment. The parameter Δ related to polyhedral distortions equals 0.04 for $Co(21)O_4$ tetrahedra (orbit 2) and 0.02 for both $Co(22)O_4$ and $Co(23)O_4$ tetrahedra (orbit 1). It can be shown that the rotational configuration obtained for the second fragment corresponds to the minimum of the elastic energy related to the polyhedra distortions. To demonstrate this, the split-atom approach developed by Giddy *et al.*[16] and Dove[18] can be applied. The approach treats each coordination polyhedron, j, as an individual molecule. The atoms that are shared by two polyhedra are treated as two distinct particles with a separation of zero. A fictitious spring of zero equilibrium length is than constructed between these split atoms and an interaction potential, $V_{jj'}(d_{jj'})$, which is harmonic with respect to the split-atom separation distance, $d_{jj'}$,

$$V_{jj'} = \frac{1}{2} K d_{jj'}^2.$$

The force constant, K, in a first approximation, represents the energy penalty associated with deformations of the polyhedra. Application of this model to the rotations of tetrahedra in the structural fragment shown in Fig. 10 gives the following expression for the split-atom harmonic potential:

$$V_{123} = V_{12} + V_{13} + V_{23} = \frac{1}{2} K(\alpha+\beta)_{12}^2 + \frac{1}{2} K(\alpha+\gamma)_{13}^2 + \frac{1}{2} K(\gamma+\beta)_{23}^2.$$

The angles α, β, and γ represent rotations of the tetrahedra with numbers in the fragment being $j=1$, 2, and 3, respectively. The angles are suggested to be small enough to consider the split-atom separation distance $d_{jj'}$ to be proportional to the corresponding tilt angles of the j and j' polyhedra. Minimization of this expression with respect of β and γ for an arbitrary fixed α gives:

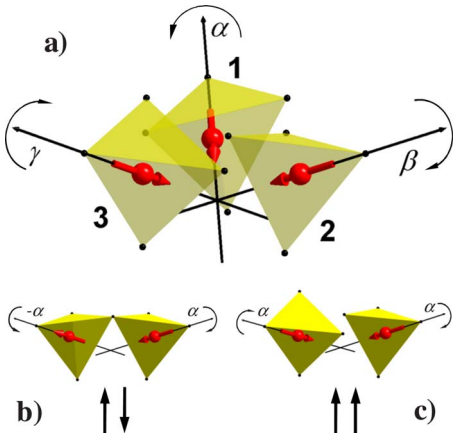

FIG. 10. (Color online) (a) Structural fragment of the kagome lattice demonstrating the split-atom approach. Tetrahedra with numbers 1, 2, and 3 rotate by angles α, β, and γ, respectively. (b) Rotations of neighbor tetrahedra without distortions (case of antiparallel pseudospins). (c) Rotations of neighbor tetrahedra with distortions (case of parallel pseudospins).

$$\left(\frac{\partial V_{123}}{\partial \beta, \gamma}\right)_{\alpha=const} = 0 \Rightarrow \beta = \gamma = -\frac{\alpha}{3}.$$

Thus, for an arbitrary rotation of the first tetrahedron, in the clockwise direction by angle α, the minimum of V_{123} corresponds to the configuration when both the second and the third tetrahedra rotate about their individual axes in anticlockwise directions by angles which are three times smaller than α. The first tetrahedron can be related to the orbit 2, whereas the second and the third ones to the orbit 1. This simple consideration gives qualitative understanding why the polyhedra in the kagome sublattice rotate in that way, i.e., why this kind of pseudovector distortion-mode condensates at the phase transition.

Considering the tetrahedra rotations as effectively coupled spins in a "pseudospin space," the obtained above result can be presented in a different way and clearly correlated with Heisenberg spins in a triangular plaquette. When neighbor polyhedra rotate without distortions (i.e., one clockwise way by an arbitrary angle α, another anticlockwise by the equal angle) it corresponds to antiparallel directions of the pseudospins [Fig. 10(b)]. When the polyhedra are tilted by the same way (both clock or anticlockwise), with associated distortions, it corresponds to the case when the pseudospins are forced to be parallel each other [Fig. 10(c)]. Any intermediate situation (one tetrahedron is tilted by an angle α and another by an angle γ, $-\alpha < \gamma < \alpha$) can be presented as a noncollinear configuration where the angle, ξ, between the pseudospins depends on the split-atom separate distance $(d_{jj'} \sim \alpha+\gamma)$ $\xi = \pi - \frac{\pi(\alpha+\gamma)}{2\alpha}$. Based on this formalism, the obtained above mutual rotations of the tetrahedra which minimize the elastic energy associated with their distortions can be interpreted as 120° configuration between the relevant pseudospins. This configuration is the well-known ground state for a triangular plaquette of Heisenberg spins. It should be pointed out that the close analogy between the classical magnetic moments and the pseudospins adapted here to rep-

resent interactions between the rotational distortions in the crystal is motivated by common symmetry reasons but not a particular form of the potential acting between spins (pseudospins). In both cases, the presence of frustration is caused by the fundamental incompatibility between threefold symmetry of the basic structural fragment (triangle) and character of the interactions between the elements of this fragment (magnetic moments or axial vectors representing polyhedral rotations). Therefore, in spite of the different nature of the interacting elements, the identical behavior can be found in both systems.

Finally, it should be pointed out that the $Pna2_1$ space group allows all three angles α, β, and γ to be different since there are no symmetry elements interchanging the corresponding sites. The stability of the configuration with two equivalent angles is not therefore a direct requirement of the space group and instead, is motivated by energetic reasons. This observation can be important when analyzing the magnetic structure of $TmBaCo_4O_7$. According to our preliminary data, long-range magnetic ordering in this composition is established below 100 K. The discussed above tilt configuration can introduce some degeneracy in exchange parameters which is not expected in the $Pna2_1$ symmetry. As a result the magnetic structure can for instance involve basis functions of more than a single irrep of the $Pna2_1$ space group.

C. Origin of the phase transformations

Starting from the "virtual" hexagonal $P6_3mc$ structure, the symmetry lowering through the complex CoO_4 polyhedral tilting down to trigonal $P31c$ and then to orthorhombic $Pna2_1$ can be most naturally attributed to the bonding requirements of Ba^{2+} and Tm^{3+} cations. The presence of strongly underbonded barium and overbonded thulium in the hexagonal structure induce the complex redistribution in the oxygen positions resulting in the observed sequence of phase transitions. This is consistent with the fact that the primary distortion modes in both phases are related to oxygen displacements which improve BVS of these cations, whereas the shifts of other cations, in particular cobalt, are ten to fifteen times smaller. This effect does not seem compatible with the magnetostrictive mechanism proposed by Maignan *et al.*,[14] because in this case a more active participation of the distortion-modes involving cobalt displacements would be expected. This especially relates to the Co-displacive modes with the M_2 symmetry, which should be primary parameters in the case of magnetostriction. Our analysis revealed that the amplitudes of these modes are very small ($\sim$0.01 Å–0.05 Å) and are practically the same as the amplitudes of the secondary modes with the higher Γ_5 and Γ_1 symmetries. Thus, the passive role of the Co-displacive modes in combination with the absence of a long-range magnetic ordering just below the $P31c \rightarrow Pna2_1$ critical temperature, $T_S \sim 240$ K (the magnetic ordering develops only below $\sim$100 K), tend to disfavor the magnetostrictive scenario. Concerning a charge ordering between Co^{3+} and Co^{2+} cations in the triangular and kagome sublattices, respectively, suggested by Nakayama *et al.*[4] as the possible mechanism of the first-order $P31c \rightarrow Pna2_1$ phase transition the following symmetry objections can be given. From a symmetry point of view, the occupancy probabilities for the Co1($2a$) and Co2($6c$) parent positions by ions with different charge state are scalar quantities which transform as the totally symmetric (identity) irreducible representation of the $P6_3mc$ space group. Thus, the corresponding order parameter is not symmetry breaking and can mediate only isostructural phase transition. From this point of view, the charge ordering may be present in the low-temperature orthorhombic phase just as a secondary order parameter via coupling with the primary one which seems to have a displacive nature. Analysis of the low-temperature structural data ($Pna2_1$ phase) revealed that the average Co1-O distance in the triangular sublattice [1.898(9)] is slightly smaller than the corresponding distances in the kagome layers (1.961(8) Å, 1.953(9) Å and 1.937(9) Å for Co21, Co22, and Co23, respectively). This can be associated with a partial charge ordering but due to the symmetry arguments mentioned above it definitely cannot be the driving force of the symmetry lowering.

V. CONCLUSION

To satisfy bonding conditions of Ba^{2+} and Tm^{3+} cations in the $TmBaCo_4O_7$, the hexagonal $P6_3mc$ symmetry is lowered initially down to trigonal $P31c$ and then to orthorhombic $Pna2_1$. In both cases, the symmetry lowering is driven by oxygen displacements which can be associated with rotations of tetrahedra coordinated around cobalt ions. The specific topology of the hexagonal structure does not allow the CoO_4 tetrahedra to rotate as rigid units resulting in their inevitable distortions. In the trigonal structure, tetrahedral units of the triangular sublattice are tilted about the c axis. These primary distortions induce small ferrodistortive rotations of CoO_4 polyhedra in the kagome layers. The passive role of the latter rotations restricts the ability of the lattice to improve the bonding conditions and results in the $P31c \rightarrow Pna2_1$ phase transformation at $T_S \sim 240$ K. The orthorhombic phase preserves the tetrahedral tilting in the triangular lattice and additionally involves rotations of polyhedra in the kagome layers about the [16,8,3], $[\bar{8},8,3]$, and $[\bar{8},1\bar{6},3]$ crystallographic axes for Co in the layer $z \sim 11/16$ and about the $[8,\bar{8},3]$, [8,16,3], and $[1\bar{6},\bar{8},3]$ axes when in the layer $z \sim 3/16$. The tetrahedral units located within a same kagome layer and rotated about the three different axes are not restricted by the $Pna2_1$ symmetry to have equivalent rotational angles, however the stable configuration which corresponds to minimum of the elastic energy related to the polyhedral distortions is when two of them are equivalent. This fact can introduce additional degeneracy into the structure which is not expected in the $Pna2_1$ symmetry and can play an important role in understanding the nature of the long-range magnetic ordered state in this class of compounds.

ACKNOWLEDGMENT

Work at Argonne supported under Contract No. DE-AC02-06CH11357 by UChicago Argonne, LLC, Operator of

Argonne National Laboratory, a U.S. Department of Energy Office of Science Laboratory.

APPENDIX

To describe the symmetry properties of the distorted phases we used the conventional group-theoretical approach. In both the trigonal and the orthorhombic phases, the primary displacive modes can be presented by pseudovector functions, $\boldsymbol{S}(\boldsymbol{r})$, localized on the cobalt positions $\boldsymbol{r}=\boldsymbol{r}_i+\boldsymbol{t}_n$; where $\boldsymbol{r}_i$—coordinates of Co ions in an unit cell and $\boldsymbol{t}_n$—lattice vector of the unit cell. This symmetry breaking part of the density function was suggested to be presented as a linear combination of symmetrized pseudovector functions, $\boldsymbol{\psi}(\boldsymbol{r})$, which transform like basis functions of a single d_ν-dimensional irrep, ν, of the hexagonal $P6_3mc$ space group.

$$\boldsymbol{S}^\nu(\boldsymbol{r}) = \sum_{\lambda}^{d_\nu} C_\lambda^\nu \boldsymbol{\psi}_\lambda^\nu(\boldsymbol{r}).$$

In a general case, the active irrep is associated with multi-arms wave-vector star, $\{\boldsymbol{k}\}$ and the basis functions are superposition of contributions from all arms, $\boldsymbol{k}_L$ $(L=1\ldots l_k)$, involved in the transition.

$$\boldsymbol{S}^{\{k\}\nu}(\boldsymbol{r}) = \sum_{L}^{l_k} \sum_{\lambda}^{l_\nu} C_\lambda^{\boldsymbol{k}_L\nu} \boldsymbol{\psi}_\lambda^{\boldsymbol{k}_L\nu}(\boldsymbol{r}).$$

The components related to a single arm, $\boldsymbol{\psi}_\lambda^{\boldsymbol{k}_L\nu}(\boldsymbol{r})$, transform like basis functions of l_ν—dimensional irreps of the wave-vector group (set of symmetry operations keeping $\boldsymbol{k}_L$ invariant or changing it into equivalent one). Irreps of the wave-vector group induce irreps of the parent group so both can be enumerated by the same symbol ν. The dimensionality of the symmetry breaking irrep of the parent group, in this case is $d_\nu=l_k\times l_\nu$. These single-arm components of the basis functions are conveniently written for a crystal with N unit cells as many-dimensional vector column:

$$\boldsymbol{\psi}_\lambda^{\boldsymbol{k}_L\nu}(\boldsymbol{r}) = \sum\nolimits_{n=1\ldots N}^{\oplus} \boldsymbol{\varphi}_\lambda^{\boldsymbol{k}_L\nu}(\boldsymbol{r}_i)\exp(i\boldsymbol{k}_L\boldsymbol{t}_n),$$

where $\boldsymbol{\varphi}_\lambda^{\boldsymbol{k}_L\nu}(\boldsymbol{r}_i)$ are 3σ-dimensional vectors constructed from atomic components, $\varphi_{i,\alpha,\lambda}^{\boldsymbol{k}_L\nu}(\boldsymbol{r}_i)$, of the basis functions, localized on a crystallographic orbit with multiplicity σ in the primary "zero" unit cell.

$$\boldsymbol{\varphi}_\lambda^{\boldsymbol{k}_L\nu}(\boldsymbol{r}_i) = \sum\nolimits_{i=1\ldots\sigma,\alpha=x,y,z}^{\oplus} \varphi_{i,\alpha,\lambda}^{\boldsymbol{k}_L\nu}\{\boldsymbol{e}_{i\alpha}\}.$$

$\{\boldsymbol{e}_{i\alpha}\}$ represent unit components of pseudovectors on atom i in the direction α.

These atomic components of the basis functions for each arm of the wave-vector star can be obtained by projection operator:

$$\hat{P}^\nu = \sum_g d_{j,\lambda}^\nu(g)T(g),$$

where the sum is taken over symmetry elements g of the little group. $d_{j,\lambda}^\nu$-matrix representation of g in irrep ν of the wave-vector group.

The operator acts on arbitrary set of pseudovector components on atoms related by symmetry operations of the wave-vector group and produces their symmetrized combination transforming like basis functions of the ν.

In the present work, we calculated atomic components of pseudovector basis functions on the Co1$(2a)$ and Co2$(6c)$ positions for some of irreducible representations associated with $\boldsymbol{k}=0$ and $\boldsymbol{k}=\boldsymbol{a}^*/2$ wave-vector groups. For the latter case, just single-arm components are of interest. The results of the calculations performed with the aid of ISOTROPY software[30] are presented in Tables III and V, respectively.

[1] R. Moessner and A. P. Ramirez, Phys. Today **59** (2), 24 (2006).
[2] D. V. Sheptyakov, A. Podlesnyak, S. N. Barilo, S. V. Shiryaev, D. D. Khalyavin, D. Yu. Chernyshov, and N. I. Leonyuk, PSI Sci. Rep. **3**, 64 (2001).
[3] M. Valldor and M. Andersson, Solid State Sci. **4**, 923 (2002).
[4] N. Nakayama, T. Mizota, Y. Ueda, A. N. Sokolov, and A. N. Vasiliev, J. Magn. Magn. Mater. **300**, 98 (2006).
[5] W. Schweika, M. Valldor, and P. Lemmens, Phys. Rev. Lett. **98**, 067201 (2007).
[6] A. Maignan, V. Caignaert, V. Pralong, D. Pelloquin, and S. Hebert, J. Solid State Chem. **181**, 1220 (2008).
[7] A. Huq, J. F. Mitchell, H. Zheng, L. C. Chapon, P. G. Radaelli, K. S. Knight, and P. W. Stephens, J. Solid State Chem. **179**, 1136 (2006).
[8] V. Caignaert, A. Maignan, V. Pralong, S. Hébert, and D. Pelloquin, Solid State Sci. **8**, 1160 (2006).
[9] A. Maignan, V. Caignaert, D. Pelloquin, S. Hebert, V. Pralong, J. Hejtmanek, and D. Khomskii, Phys. Rev. B **74**, 165110 (2006).
[10] M. Soda, T. Moyoshi, Y. Yasui, M. Sato, and K. Kakurai, J. Phys. Soc. Jpn. **76**, 084701 (2007).
[11] M. Soda, Y. Yasui, T. Moyoshi, M. Sato, N. Igawa, and K. Kakurai, J. Magn. Magn. Mater. **310**, e441 (2007).
[12] M. Soda, Y. Yasui, T. Moyoshi, M. Sato, N. Igawa, and K. Kakurai, J. Phys. Soc. Jpn. **75**, 054707 (2006).
[13] L. C. Chapon, P. G. Radaelli, H. Zheng, and J. F. Mitchell, Phys. Rev. B **74**, 172401 (2006).
[14] A. Maignan, S. Hebert, V. Caignaert, V. Pralong, and D. Pelloquin, Solid State Commun. **147**, 470 (2008).
[15] A. M. Glazer, Acta Crystallogr. B **28**, 3384 (1972).
[16] A. P. Giddy, M. T. Dove, G. S. Pawley, and V. Heine, Acta Crystallogr. A **49**, 697 (1993).
[17] M. T. Dove, M. Gambhir, K. D. Hammonds, V. Heine, and A. K. A. Pryde, Phase Transit. **58**, 121 (1996).
[18] M. T. Dove, Am. Mineral. **82**, 213 (1997).
[19] M. T. Dove, M. J. Harris, A. C. Hannon, J. M. Parker, I. P. Swainson, and M. Gambhir, Phys. Rev. Lett. **78**, 1070 (1997).
[20] We do not mean the cases when the driving force for a phase transformation is an electronic instability of transition metals

inside the polyhdera, such as for instance Jahn-Teller effect or ferroelectric/antiferroelectric displacements.
[21] A. M. Glazer, Acta Crystallogr. A **31**, 756 (1975).
[22] C. J. Howard and H. T. Stokes, Acta Crystallogr. B **54**, 782 (1998).
[23] C. J. Howard, B. J. Kennedy, and P. M. Woodward, Acta Crystallogr. B **59**, 463 (2003).
[24] P. M. Woodward, Acta Crystallogr. B **53**, 32 (1997).
[25] J. C. Maxwell, Philos. Mag. **27**, 294 (1864).
[26] K. D. Hammonds, A. Bosenick, M. T. Dove, and V. Heine, Am. Mineral. **83**, 476 (1998).
[27] J. Rodríguez-Carvajal, Physica B **192**, 55 (1993).
[28] D. M. Hatch and H. T. Stokes, Phys. Rev. B **31**, 2908 (1985).
[29] H. T. Stokes and D. M. Hatch, *Isotropy Subgroups of the 230 Crystallographic Space Groups* (World Scientific, Singapore, 1988).
[30] H. T. Stokes and D. M. Hatch, ISOTROPY, 2000, http://stokes.byu.edu/isotropy.html
[31] S. C. Miller and W. F. Love, *Tables of Irreducible Representations of Space Groups and Co-Representations of Magnetic Space Groups*, 4th ed. (Preutt Press, Boulder, 1967).
[32] B. J. Campbell, H. T. Stokes, D. E. Tanner, and D. M. Hatch, J. Appl. Crystallogr. **39**, 607 (2006).
[33] Individual displacive modes of parent ions are identified with the labels of the form: irrep [parent atom: Wyckoff site] point group irrep that breaks the local site symmetry and (the branch of the order parameter). For details see Ref. 32.
[34] R. H. Mitchell, *Perovskites: Modern and Ancient* (Almaz Press, Thunder Bay, ON, 2002).